

The Concept Allocation Zone

Tracking How Concepts Form Across Transformer Depth

James Henry

Independent Researcher · jamesrahenry@henrynet.ca · ORCID 0009-0005-7126-9466

May 12, 2026

Abstract

Concept formation in transformer language models is a depth-extended process, not a single-layer event: concepts emerge gradually across a contiguous region of the residual stream and settle only after their primary assembly phase is complete. Mechanistic interpretability methods commonly extract concept representations by identifying the single optimal layer of a Transformer’s residual stream where class separation peaks. This “best layer” heuristic is computationally efficient and empirically grounded, but it captures a snapshot of a process rather than the process itself. We introduce the **Concept Allocation Zone** (CAZ): a region of model depth allocated to the geometric expression of one or more concepts — the interval within which a concept becomes measurably separable. CAZ frames concept allocation as a depth-extended phenomenon and surfaces structure that single-layer methods do not include. We formalize the CAZ through three layer-wise metrics — Separation, Concept Coherence, and Concept Velocity — and derive principled methods for identifying CAZ boundaries without manual layer sweeps. A CAZ is not a concept: it is the depth region within which a computational event occurs — the model organizing its geometry to make a concept measurably separable. Multiple concepts may share a CAZ, and a single concept typically participates in multiple CAZes across depth. Empirical validation across 34 models from 8 architectural families and 7 concepts reveals that the separation curve $S(l)$ is frequently **multimodal**, with a scored detection method uncovering an additional category of subtle allocation regions (“gentle CAZes”) that are invisible to standard peak detection but are causally active (as measured by ablation-induced geometric separation reduction; behavioral pilot in [Henry, 2026c] §6.8) in 93–100% of cases across models with full ablation coverage (16 of 34 models in this analysis; 26 base models in the companion evaluation [Henry, 2026c]; under the current 0.5% prominence floor; see §4.3). The framework generates seven testable predictions; all seven were evaluated — four yield clear verdicts (two not supported, one partially supported, one supported), one had its precondition invalidated by the data (P4), and two are underpowered (P3 — exploratory, $n = 6$ concepts; P7 — indeterminate, insufficient scale ladder) — with cross-architecture alignment confirmed as depth-matched rather than monolithic under leave-one-concept-out cross-validation. The reference implementation is provided in the open-source `rosetta_tools` library (v1.3.1) [Henry, 2026].

1. Introduction

The dominant paradigm in mechanistic interpretability extracts concept representations by identifying the single “best layer”—the residual stream depth at which a linear probe or difference-of-means (DoM) vector achieves maximum class separation [Zou et al., 2023; Arditi et al., 2024]. This heuristic is computationally convenient and empirically grounded. It is also, by design, a snapshot: it identifies the peak of a process rather than characterizing the process itself.

arXiv:2605.24856v1 [cs.LG] 24 May 2026

Transformers are iterative dynamical systems. Each layer applies a sequence of attention and MLP operations that *write* new information into the residual stream, modifying and extending what prior layers contributed [Elhage et al., 2021]. A concept observed at Layer 15 was shaped by Layers 10 through 14 before it; the best-layer heuristic tells us where the concept is most legible, not how it arrived there.

This paper introduces the **Concept Allocation Zone** (CAZ) framework, which extends the interpretability toolkit from anatomy—*where is the concept most visible?*—to dynamical flow—*how does the concept form?* The CAZ is defined as a region of model depth allocated to the geometric expression of a concept — the interval within which that concept becomes measurably separable. A CAZ is not the concept itself — each CAZ is a depth-localized region of the residual stream in which the model’s geometry expresses influence to serve a concept.

The framework has immediate practical implications:

1. **Richer extraction.** CAZ-windowed extraction methods may capture information present in the allocation dynamics that single-layer methods do not.
2. **Principled intervention.** Ablation at different points in the CAZ chain produces qualitatively different effects. The framework provides a geometric basis for selecting intervention depth.
3. **Dark matter connection.** The structured residual left unexplained by sparse autoencoders [Engels et al., 2025a] may partially correspond to in-progress concept construction within CAZes — transitional representations that resist linear decomposition at any single layer. This is a testable hypothesis; direct cross-validation of CAZ regions against SAE residuals has not been conducted in this work.
4. **Cross-model transfer.** Concept directions can be depth-matched across architectures — the mechanism enabling transferable interpretability tooling. Whether a single Procrustes rotation suffices to align all concepts simultaneously is the subject of the companion PRH paper [Henry, 2026d], published simultaneously with this work.
5. **Understanding alignment training.** CAZ profiles provide a lens for studying what preference optimization changes in a model — not whether concepts exist, but where and how they are allocated. Empirical comparison of 8 base/instruct model pairs in the companion validation paper [Henry, 2026c], published simultaneously with this work, reveals that instruction tuning does not uniformly shift concept allocation to shallower depths; the direction and magnitude of change depend on the base model’s existing concept geometry. This provides a CAZ-based metric for quantifying alignment training distortion: the change in concept-selective feature count and alignment strength from base to instruct variant.
6. **Concept inventory.** By tracking which geometric directions are allocated at each CAZ and which remain unaligned with any human concept probe, the framework provides a systematic approach to cataloguing what a model computes — both the named and the unnamed.

The CAZ framework generates specific, falsifiable predictions. Section 5 evaluates all seven predictions across 34 models and 8 architectural families — four yield clear verdicts (two not supported, one partially supported, one supported), one had its precondition invalidated by the data (P4), and two are underpowered. The framework’s strongest empirical result is a depth-stratified refinement of the Platonic Representation Hypothesis: cross-architecture alignment is matched by processing depth rather than by architecture as a whole, a result confirmed under leave-one-concept-out cross-validation (§5.5). The reference implementation is provided as `rosetta_tools` [Henry, 2026], an open-source Python library. We are explicit about the assumptions the framework inherits from the broader interpretability literature.

Corpus and analysis coverage. Each companion paper uses a model set scoped to its analysis; the table below records the scope rationale for each:

Analysis	Coverage	Scope rationale
CAZ detection and predictions (this paper)	34 models, 7 concepts	26 base + 8 instruct; full architectural range
Direction-specificity ablation (this paper)	16 of 34 models	Extended to all 26 base models in [Henry, 2026c]
GEM handoff validation [Henry, 2026b]	23 base models, 17 concepts	Base models only; concept set expanded for handoff analysis
Full ablation sweep [Henry, 2026c]	26 base models, 7 concepts	Instruct variants excluded; systematic per-prediction evaluation

2. Relationship to Existing Work

The CAZ framework operates in the same space as several established interpretability methods. Each captures different aspects of model internals; the CAZ contribution is the layer-indexed dynamical view — tracking *when* representations form, not just *what* they are.

2.1 Methodological Context

Logit Lens and Tuned Lens. The most direct methodological antecedents of the CAZ framework are the logit lens [nostalgebraist, 2020] and the tuned lens [Belrose et al., 2023]. Both project intermediate residual-stream activations into a fixed interpretive space — the unembedding matrix for logit lens, a per-layer trained affine probe for tuned lens — to produce a layer-by-layer trajectory of the model’s evolving prediction. CAZ shares the core commitment to tracking representations across depth rather than characterizing a single best layer, and any claim about layer-indexed concept dynamics necessarily inherits from this line of work. The distinction is what is being projected and asked. Logit and tuned lens project onto output-vocabulary space and ask *what token would this layer predict if the model stopped here?*; the CAZ framework projects onto concept-contrast directions obtained from external stimulus pairs and asks *where in the stack is this concept being allocated?* Concepts without a canonical lexicalization — credibility, refusal, moral valence — do not project cleanly onto vocabulary axes and fall outside the natural scope of logit-lens interpretation, which motivates the contrast-direction formulation used here. Calibrating the velocity metric against Tuned Lens in settings where concept and vocabulary are tightly coupled is left to future work.

Sparse Autoencoders (SAEs) decompose activations at a fixed layer into interpretable monosemantic features [Cunningham et al., 2023; Bricken et al., 2023]. SAEs answer “what features exist at layer L?” The CAZ framework answers “how does the feature at layer L relate to the feature at layers L−1 and L+1?” The approaches are complementary: SAE features at a given layer are a snapshot; CAZ tracking reveals which snapshots are part of the same evolving computation. Engels et al. [2025a] found that SAE “dark matter” — structured residual that resists linear decomposition — accounts for roughly 50% of the error vector. The CAZ framework offers a candidate mechanism: in-progress concept construction within a CAZ produces transitional representations that are neither the input feature nor the output feature. These transitional states may be precisely what resists decomposition at any single layer.

Centered Kernel Alignment (CKA) [Kornblith et al., 2019] measures representational similarity between layers or models by comparing activation kernel matrices. CKA provides a global similarity score between two representation spaces but does not identify *which* features are shared or how they evolve across depth. The CAZ framework tracks individual concept directions layer by layer, producing a trajectory rather than a scalar comparison. Whether CKA serves as a complementary validation tool — high within a CAZ where the representation is being refined, low at inter-CAZ saddle points where it is being reallocated — is left to future work.

Linear probing [Belinkov, 2022; Alain & Bengio, 2017] trains classifiers on activations at each layer to measure concept presence. Probing accuracy curves are closely related to the separation metric $S(l)$ — both measure how distinguishable two classes are at a given depth. The CAZ framework adds the velocity metric (rate of change of separation) and the coherence metric (geometric quality of the separating direction) — formalized in §4 — which together identify not just where a concept is present but where it is actively being constructed. Probing also requires training a classifier per layer; the CAZ metrics are computed directly from activation statistics.

Representation Engineering (RepE) [Zou et al., 2023] extracts concept directions for honesty, morality, power-seeking, and related concepts via contrastive stimuli, then uses those directions for monitoring and steering. The CAZ framework can directly inform RepE’s operational decisions. First, the CAZ profile identifies where a concept is being actively constructed versus where it is established, providing a principled basis for choosing intervention depth. Second, the model’s encoding strategy determines whether layer selection matters at all: in models with redundant encoding, the concept direction persists across all post-CAZ layers, so RepE can intervene anywhere with equivalent effect. In models with sparse encoding, the CAZ peak is the critical intervention point and intervening elsewhere may miss the target. Third, the scored CAZ detector (§4) reveals that a concept may have multiple intervention-worthy layers — RepE steering applied at a gentle CAZ (§4) may produce different behavioral effects than steering at the dominant peak.

Activation patching and causal scrubbing. Activation patching — replacing activations at a specified layer and component with those from a counterfactual run [Vig et al., 2020; Meng et al., 2022; Wang et al., 2023] — is the canonical toolkit for testing whether a proposed locus genuinely carries a computation. Causal scrubbing [Chan et al., 2022] formalizes this as a discipline for rigorously testing mechanistic hypotheses; path patching [Goldowsky-Dill et al., 2023] extends the method to circuit-level attribution. Any claim of the form “the concept is allocated at layer l ” is a candidate for validation under this family of methods, and the ablation protocol used in the companion paper [Henry, 2026c] is a direct descendant. The CAZ contribution is upstream of patching rather than parallel to it: the velocity-based boundary and score-based region detectors (§4) produce a principled, concept-specific choice of *which* layers to patch, replacing exhaustive layer sweeps with a targeted hypothesis about the allocation zone. The two methods are therefore complementary — CAZ identifies candidate layers; activation patching tests whether the identified layers are causally necessary.

2.2 Related Empirical Findings

MLP feed-forward layers as key-value memories. Geva et al. [2021, 2022] showed that FFN layers function as key-value memories that incrementally promote concepts into the vocabulary space across depth. The CAZ metrics ($S(l)$, $v(l)$, $C(l)$) are defined on the residual stream and are agnostic to whether promotion happens through attention or feed-forward paths; connecting CAZ boundaries to specific FFN write operations is a testable mechanistic question not pursued here.

Manifold interpretability. Gurnee et al. [2026] found curved manifolds in middle layers for character counting and explicitly called for unsupervised geometric discovery methods. The CAZ framework provides a formalism for identifying *where* in the layer stack such manifolds crystallize — the allocation zone is precisely where curved manifold structure should be most geometrically coherent.

The geometry of refusal. Arditi et al. [2024] and Wollschläger et al. [2025] establish the geometric structure of refusal — a single removable direction (ablation) and multi-dimensional concept cones, respectively. The CAZ framework extends this by asking not just *what* the geometry is but *when* it forms, and using that temporal structure to identify optimal intervention points.

Multi-dimensional concept structure. Engels et al. [2025b] found circular multi-dimensional representations for temporal concepts that are not decomposable into independent one-dimensional SAE features. Wollschläger et al. [2025] showed refusal occupies polyhedral concept cones. These findings establish that rich geometric structure exists; the CAZ framework provides a layer-indexed account of when such structures crystallize.

Concept geometry in production models. Sofroniew et al. [2026] demonstrate that Claude Sonnet 4.5 develops internal representations of 171 emotion concepts whose geometry is stable across model depth (particularly early-middle to late layers) and generalizes across contexts and behaviors. The representations causally influence model behavior — including downstream effects on reward hacking, sycophancy, and blackmail — confirmed via activation steering. Concept vectors are extracted by averaging residual stream activations across stories per emotion and subtracting the cross-emotion mean; the resulting representations cluster by semantic similarity with valence and arousal as primary axes, mirroring human psychological structure. This result provides direct peer-reviewed support for two foundational claims underlying the CAZ framework: that transformers develop stable, generalizable geometric representations of human-interpretable concepts in their residual streams — representations that hold across diverse inputs rather than being probe artifacts — and that this structure is causally meaningful rather than a mere correlate of surface features.

The Platonic Representation Hypothesis. Huh et al. [2024] proposed that models trained on different data and architectures converge on shared representations. The CAZ framework enables a depth-stratified test of this hypothesis: rather than measuring global alignment, we can ask whether convergence differs at shallow versus deep processing stages.

Universal neurons. Gurnee et al. [2024] identified individual neurons in GPT-2 that activate on consistent input features across five independent training runs — direct evidence that specific representational structure is stable under retraining. This is a neuron-level instantiation of the architectural-convergence phenomenon the Platonic Representation Hypothesis [Huh et al., 2024] addresses at the level of whole representation spaces. The CAZ framework predicts a depth-stratified extension of both claims: if concepts allocate at architecturally-stable proportional depths, then the layers hosting universal neurons for a given concept should correspond to that concept’s CAZ peak in proportional terms, and cross-architecture alignment of concept directions should be strongest when evaluated at matched CAZ depths rather than at matched absolute layer indices. Universal-neuron discovery and CAZ-profile matching are therefore two lenses on the same underlying regularity at different granularities.

3. Background

3.1 The Residual Stream and Concept Representation

The residual stream formulation [Elhage et al., 2021] treats each layer’s output as an additive contribution to a shared communication channel. Attention heads and MLPs read from and write to this stream; the final residual vector is projected onto the unembedding matrix to produce logits. This architecture makes layer-by-layer tracking of concept geometry natural: we can ask, at each layer l , how well the current residual stream separates two contrastive classes.

3.2 Difference-of-Means and Linear Artificial Tomography

DoM extracts a concept direction $V_{\text{concept}} \in \mathbb{R}^d$ as the normalized difference between class-conditional mean activations at the chosen layer [Zou et al., 2023]. Linear Artificial Tomography (LAT) uses a similar contrastive approach. Both methods produce a single vector at a single depth—a precise and useful representation of where the concept is most geometrically legible. The CAZ framework asks what additional information about concept formation might be recoverable from the layers surrounding that peak.

3.3 Abliteration and Intervention Depth

Arditi et al. [2024] demonstrated that refusal behavior across 13 open-source models is mediated by a single direction removable via weight orthogonalization (“abliteration”). Independent replications have observed KL divergences between abliterated and unmodified models ranging from 3.16 to 5.71 — suggesting that while behavioral suppression is effective, the intervention also affects general model capabilities. The CAZ framework motivates a systematic study of intervention depth: rather than selecting a single layer by hyperparameter search, the CAZ profile identifies where concepts are being actively constructed versus where they are established, offering a principled basis for choosing intervention points (Section 5.1).

3.4 The Emerging Geometric Program

Gurnee et al. [2026] demonstrated that character counts are represented on low-dimensional curved helical manifolds in the residual stream, with attention heads performing geometric transformations on these structures. Engels et al. [2025b] found circular multi-dimensional representations for temporal concepts (days, months, years) that are not decomposable into independent one-dimensional SAE features. Wollschläger et al. [2025] showed that refusal occupies multi-dimensional polyhedral concept cones with multiple independent directions. These findings establish a growing body of evidence for rich geometric structure in activation space, and have explicitly called for unsupervised methods to detect and characterize it. The CAZ framework is designed to complement this geometric program by providing a layer-indexed account of when such structures crystallize.

4. The Concept Allocation Zone

A CAZ is not a concept. It is a region of model depth allocated to the geometric expression of one or more concepts — the depth interval within which a concept becomes measurably separable. The concept is the human label we project onto the geometry; the CAZ is the interval of depth where that geometry is organized. A single CAZ may host multiple concepts simultaneously ([Henry,

2026c]), and a single concept typically participates in multiple CAZes across depth (mean 3.4 per concept per model; [Henry, 2026c]). The distinction matters: when we say “credibility has a CAZ at layer 10,” we mean that layer 10 falls within a depth interval allocated to credibility’s geometric expression — not that layer 10 “contains” credibility.

Terminology

Term	Definition
CAZ	A depth-localized region of the residual stream where the model organizes geometry to serve a concept
CAZ Profile	The full sequence of CAZes for one concept in one model
Major CAZ	CAZ with score > 0.5 — high-prominence, concentrated allocation region
Strong CAZ	CAZ with score 0.2–0.5
Moderate CAZ	CAZ with score 0.05–0.2
Gentle CAZ	Subtle CAZ with score < 0.05 — causally active but invisible to standard detection
Embedding CAZ	CAZ at the embedding boundary, driven by token-level features rather than transformer computation
Active CAZ	CAZ within the transformer layers, driven by attention and MLP computation. Active CAZes are the primary subject of this framework
CAZ score	Composite metric: prominence \times coherence boost $\times \sqrt{\text{width}}$
Separation $S(l)$	Fisher-normalized centroid distance between contrastive classes at layer l
Coherence $C(l)$	Explained variance ratio of the primary separating direction at layer l
Velocity $v(l)$	Smoothed rate of change of $S(l)$ across layers
Directional stability $DS(l)$	Layer-to-layer cosine similarity of the dominant concept direction $\hat{d}(l)$; near 1.0 means the direction barely moved; a sharp drop marks a handoff (§4.2, GEM paper [Henry, 2026b])

4.1 Concept Lifecycle

By tracking the residual stream across model depth, concept formation is empirically distinguishable as a sequence of allocation regions rather than a single allocation followed by decay.

Early layers (Context and Syntax)

In early layers, the residual stream primarily resolves local context, grammar, and surface token relationships. Projecting contrastive datasets into this space generally produces heavily entangled activations; the separation metric is near zero. The model has not yet committed to a semantic trajectory.

However, the scored detector does find CAZes at layers 0–1 in tens of concept \times model pairs across the validation corpus — concentrated in concepts with strong lexical cues such as negation and credibility, with the precise per-model breakdown reported in the companion validation paper [Henry, 2026c]. Most are gentle (score < 0.1) and reflect **embedding leakage** — concept-associated tokens having distinctive embeddings that create passive separation before any transformer processing occurs. We term these **embedding CAZes** to distinguish them from **active CAZes** where the model’s attention and MLP computations allocate geometry to serve a concept. The embedding CAZ signal is a property of the tokenizer and training corpus, not a computational decision by the model. Practitioners using CAZ profiles should be aware that embedding CAZes may not respond to the same interventions as active CAZes.

CAZ Chain (Concept Allocation)

As the residual stream deepens, geometric directions are allocated to concepts in contiguous depth regions — the CAZes. A persistent direction in activation space may serve one concept at shallow layers, be reallocated to a different concept at a mid-depth CAZ, and reallocated again at a deeper one. Cross-concept direction sharing is common at specific depth regions: independent SAE cross-validation identifies four layer positions each hosting six of seventeen concept eigenvectors simultaneously — direct evidence of bandwidth reuse ([Henry, 2026c]). The most universal features across architectures are those that rotate through multiple concept alignments across depth. For a given concept, the separation metric $S(l)$ reflects when that concept holds a strong claim on one or more geometric directions. A single concept typically participates in multiple CAZes (mean 3.4 per concept per model under scored detection; [Henry, 2026c]), ranging from major CAZes (score > 0.5) to subtle allocation regions (“gentle CAZes,” score < 0.05) that are nonetheless causally active in 93–100% of cases across models with full ablation coverage [Henry, 2026c].

Late layers (Logit Projection)

In the final layers, the model transitions from abstract representation to concrete next-token prediction. The residual stream is projected toward the unembedding matrix. Concept geometry may degrade or re-entangle as abstract directions give way to vocabulary-specific structure. This is the only phase where separation genuinely decays — earlier apparent “decay” between CAZ peaks is better understood as reallocation of the direction to a different concept.

4.2 Layer-Wise Metrics

Let $h_l^{(i)} \in \mathbb{R}^d$ be the residual stream activation at layer l for sample i , and let A, B be contrastive classes with conditional means $\bar{h}_A^{(l)}, \bar{h}_B^{(l)}$ and within-class covariance matrices $\Sigma_A^{(l)}, \Sigma_B^{(l)}$.

Separation Metric

We define the separation at layer l using a Fisher-normalized criterion [Bishop, 2006, §4.1.4]:

$$S(l) = \frac{\|\bar{h}_A^{(l)} - \bar{h}_B^{(l)}\|_2}{\sqrt{\frac{1}{2} (\text{tr}(\Sigma_A^{(l)}) + \text{tr}(\Sigma_B^{(l)}))}}$$

In plain terms: separation asks “if I gave you a sentence and asked whether it expresses credibility or not, how easily could you tell from the model’s internal state at this layer?” A high $S(l)$ means the model’s activations for credible and non-credible text have moved far apart relative to how

spread out each group is. A low $S(l)$ means the two groups are still jumbled together. Tracking $S(l)$ across layers reveals where the model begins to “make up its mind” about a concept.

Raw centroid distance is misleading when cluster dispersion varies across layers. Early layers tend toward diffuse, high-variance representations; normalization by within-class spread corrects for this. Mahalanobis distance [Mahalanobis, 1936] would account for full covariance structure but is numerically unstable without regularization in high-dimensional activation spaces. Fisher normalization provides the appropriate tradeoff between geometric fidelity and computational feasibility for initial experiments. We use it for three concrete reasons: it admits closed-form computation with no per-layer training, it is monotone with linear separability under Gaussian class assumptions [Fisher, 1936], and it remains numerically stable in high-dimensional activation spaces without regularization. Probe accuracy curves — linear classifiers trained on the normalized directions and evaluated on held-out contrastive pairs — are reported in the companion paper as a robustness check [Henry, 2026c].

Concept Coherence

Separation alone is insufficient: two classes could exhibit identical centroid separation while one forms a tight cluster and the other a diffuse cloud. We track Concept Coherence as the explained variance ratio of the first principal component of the full pooled activation matrix at each layer:

$$C(l) = \frac{\lambda_1^{(l)}}{\sum_i \lambda_i^{(l)}}$$

where $\lambda_i^{(l)}$ are the eigenvalues of the covariance of all activations — positive and negative class combined — at layer l . Concretely, $C(l)$ is computed by fitting PCA on the concatenated $[h_A; h_B]$ matrix and reading off the explained variance ratio of the first principal component. A high $C(l)$ means the dominant source of variation across both classes is a single direction — the representation is geometrically concentrated. A low $C(l)$ means variation is spread across many dimensions — the representation is diffuse. A concept is *well-formed* when both $S(l)$ and $C(l)$ are high: the classes are far apart *and* the separating direction is geometrically clean.

In plain terms: coherence asks “is the concept encoded as a single clean direction, or is it smeared across many dimensions?” A high $C(l)$ means the dominant source of variance in the pooled activations is concentrated on a single direction — the concept has crystallized into a sharp geometric feature. A low $C(l)$ means variation is spread across multiple directions. **Precision note:** because $C(l)$ is fitted on the pooled (both-class combined) activation matrix, it measures the dominant direction of total variance, which may correspond to within-class spread rather than between-class separation. $C(l)$ is most interpretable in combination with $S(l)$: high $C(l)$ with high $S(l)$ confirms the dominant pooled direction is also the class-separating direction; high $C(l)$ with low $S(l)$ indicates activation concentration on a direction that is not class-discriminative.

Concept Velocity

To identify CAZ boundaries, we compute the rate of geometric divergence between layers. Because raw layer-to-layer differences are noisy, we smooth over a window of half-width k . The resulting sum telescopes to a finite-difference slope across the window:

$$v_{\text{concept}}(l) = \frac{S(l+k) - S(l-k-1)}{2k+1}$$

where k is the smoothing half-window. This is the slope of S between the two boundary layers of the smoothing window — equivalent to fitting a secant line across $2k + 1$ steps. A practical heuristic is $k = \max(1, \lfloor L/24 \rfloor)$, where L is total model depth. The $\max(1, \cdot)$ floor ensures at least one layer of smoothing for all models, including shallow ones (e.g., GPT-2, 12 layers, where $\lfloor 12/24 \rfloor = 0$). This yields $k = 1$ for models up to 47 layers, $k = 2$ for 48-layer models, and $k = 3$ for 72-layer models. This scales the smoothing window proportionally to model depth and prevents false CAZ boundary detection from single anomalous layers. The appropriate value of k should ultimately be determined empirically — for models where ground-truth concept boundaries can be established via ablation, the k value that maximizes boundary prediction accuracy is preferred.

In plain terms: velocity asks “is the concept forming right now, or has it already formed?” Positive velocity means separation is increasing — the model is actively constructing the concept at this layer. Negative velocity means separation is decreasing — the concept is being degraded or reallocated. Zero velocity means nothing is changing. The velocity curve marks the boundaries of the CAZ: it goes positive when allocation begins and negative when it ends.

Directional Stability

The three metrics above track *how strongly* a concept is expressed. $DS(l)$ tracks *which direction* it occupies. Let $\hat{d}(l)$ be the normalized dominant direction (`dom_vector`) at layer l — the unit vector from negative to positive class centroid. Directional stability is:

$$DS(l) = \hat{d}(l) \cdot \hat{d}(l - 1)$$

$DS(l)$ near 1.0 means the dominant direction barely moved between consecutive layers; the model is encoding the concept stably. A sharp drop marks a **handoff** — a layer at which the geometric basis of the concept shifts substantially. The Geometric Evolution Map (GEM) framework [Henry, 2026b] tracks these handoffs to identify the first post-CAZ layer where $DS(l)$ recovers, extracting the *settled* direction from that layer. The GEM angular velocity $\omega(l) = 1 - |DS(l)|$ is the complement, using the absolute value to treat direction-sign ambiguity as zero rotation rather than full rotation.

$DS(l)$ is conceptually independent from $S(l)$: separation can be high while the direction is still rotating (during active CAZ assembly), and separation can be low while the direction is stable (between concept peaks). The two signals decompose model activity into *what* is being encoded and *how stably*, respectively.

4.3 CAZ Boundary Detection

Single-Region Detection (Velocity-Based) When the $S(l)$ curve is unimodal, CAZ boundaries are derived from the velocity profile:

- **CAZ Entry** (l_{start}): The first layer where $v_{\text{concept}}(l)$ exceeds a sustained positive threshold $\theta_+ = 0.5 \times \max_l v(l)$, maintained for at least two consecutive layers.
- **CAZ Peak** (l_{max}): The layer where $S(l)$ reaches its absolute maximum. This corresponds to the “best layer” of conventional interpretability.
- **CAZ Exit** (l_{end}): The layer where $v_{\text{concept}}(l)$ becomes consistently negative for at least two consecutive layers, marking the onset of post-CAZ degradation. Note: $\theta_+ = 0.5 \times \max_l v(l)$ uses the global maximum of $v(l)$ across all layers of the model, including any negative-velocity portions.

The conventional best-layer heuristic extracts V_{concept} at l_{max} . CAZ-aware extraction uses the full interval $[l_{\text{start}}, l_{\text{end}}]$.

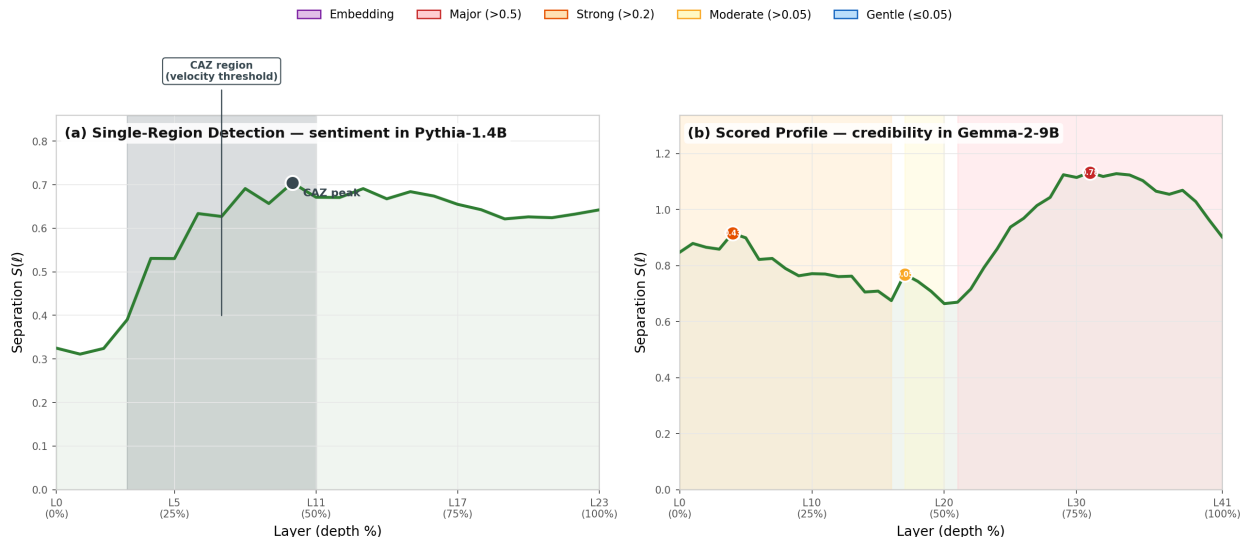


Figure 1: Single-region detection (left) versus scored CAZ profile (right). The single-region detector identifies one allocation zone for sentiment in Pythia-1.4B (peak L10, 43% depth). The scored detector reveals two strong CAZes for credibility in Gemma-2-9B — geometrically distinct sub-representations at shallow and deep processing depths (§4.5). The single-region method applied to Gemma-2-9B would report a single zone around the dominant peak; the scored detector surfaces both. Both runs: $N=250$ contrastive pairs, $k = \max(1, \lfloor L/24 \rfloor)$ smoothing, final-token probing, scored detection defaults (0.5% prominence floor, 3% valley-merge threshold).

Multi-Region Detection (CAZ Profiles) Empirical analysis across 34 models reveals that the $S(l)$ curve is frequently **multimodal** — a single concept can produce multiple significant local maxima at different depths. In these cases, the velocity-based boundary detector wraps a single contiguous zone around the global maximum and is blind to secondary peaks.

The **CAZ Profile** generalizes the single-region CAZ to a sequence of allocation regions:

1. Detect all significant local maxima in $S(l)$ using prominence-based peak detection.
2. Identify **saddle points** — the local minima between consecutive peaks — as natural region boundaries.
3. Each region spans from one saddle to the next, with the first region starting at layer 0 and the last ending at the final layer.

A CAZ Profile is characterized by: - **n_regions**: Number of distinct allocation regions (1 = unimodal, 2+ = multimodal) - **peak region**: The region with the highest peak separation - Per-region: start, peak, end, width, peak separation, coherence, rise/fall asymmetry

Scored Detection The prominence-based detector requires a threshold to determine which peaks are significant. A fixed threshold (e.g., 10% of global max separation) is arbitrary and risks discarding subtle but causally active allocation regions. We replace it with a composite scoring system:

$$\text{CAZ score} = \frac{\text{prominence}}{\bar{S}} \times \left(1 + \frac{C(l_{\text{peak}})}{\bar{C}}\right) \times \sqrt{\frac{\text{width}}{L}}$$

where **prominence** is the scipy peak-prominence value — the height of the peak above the higher of its two surrounding saddle points — with a floor of 0.5% of the global maximum $S(l)$; \bar{S} is the global mean separation across all layers; $C(l_{\text{peak}})$ is the coherence at the peak layer; \bar{C} is the global mean coherence across all layers; width is the region’s layer count; and L is total model depth. The three factors have natural interpretations: the first normalizes prominence by the baseline signal level; the second (coherence boost) rewards peaks with above-average geometric organization, with a peak at the model-wide mean coherence scoring 2.0; the third rewards wider, more sustained regions while preventing broad shallow regions from dominating. The 0.5% floor was an initial empirical choice rather than a derived threshold; post-hoc ablation across detected gentle CAZes shows 93–100% causal impact when suppressed (16 of 34 models in this analysis; 26 base models in [Henry, 2026c]), consistent with the floor admitting predominantly causal regions rather than noise. This is an upper-bound calibration: it confirms the floor is not too permissive, but does not establish whether it is too conservative — regions below the floor may also be causally active, and lower-bound calibration is open work. The scored detector is the primary detection method; the fixed-threshold detector is retained for backward compatibility.

4.4 Multi-Layer Concept Extraction

The CAZ framework motivates the question: given that a concept assembles across multiple layers, where is the best layer to extract its probe direction? Three candidate methods are:

1. **Delta PCA:** PCA on layer-to-layer residual deltas $\Delta h_l = h_l - h_{l-1}$ within $[l_{\text{start}}, l_{\text{end}}]$. This captures what each layer *adds*—the construction process itself.
2. **Windowed PCA:** PCA on raw activations h_l across $[l_{\text{start}}, l_{\text{end}}]$. This captures the cumulative concept direction as it evolves through the allocation zone.
3. **Single-layer (baseline):** The standard DoM vector at l_{max} .

Geometric Evolution Maps (GEM) provide the answer validated in the companion GEM paper [Henry, 2026b], published simultaneously with this work. GEM tracks the directional trajectory of a concept through the residual stream — specifically, the layer-to-layer angular velocity of the concept’s dominant separating direction — and identifies the *handoff layer*: the first post-CAZ layer at which angular velocity drops below a threshold and the concept direction locks into a stable encoding. The core finding is that concept probe directions undergo substantial rotation *within* the CAZ (mean entry-to-exit cosine similarity of 0.233 across 23 models from the GEM corpus [Henry, 2026b] and 17 concept types), and do not settle until a characteristic post-CAZ depth. Probing at the handoff layer — where the concept direction has stabilized — is at least as precise as peak-layer extraction in 259/391 concept \times model trials (23 models \times 17 concepts; 66.2%; Wilcoxon signed-rank $p = 3.21 \times 10^{-17}$, one-sided; trial-level); model-level Wilcoxon $W=214$, $N=23$, $p = 0.010$. The architecture cohort breakdown is pronounced: 11 of 13 MHA models prefer handoff on a strict majority of concepts versus 2 of 7 GQA models (Fisher’s exact, one-sided $p = 0.022$). Both extraction layers yield valid concept directions; which is more precise depends on architecture and on whether the concept’s separating direction undergoes meaningful rotation between peak and handoff. The CAZ profile predicts which case applies before extraction. The pattern follows the attention-mechanism cohort:

Cohort	n	Prefer handoff ($\geq 9/17$ concepts)	Prefer peak	Handoff rate
MHA	13	11: Pythia 160m, 410m, 1b, 1.4b, 2.8b, 6.9b, 12b; OPT-1.3b, OPT-6.7b; GPT-2-large, GPT-2-XL	2: Pythia-70m, GPT-2	85%
GQA	7	2: Mistral-7B-v0.3, Llama-3.1-8B	5: Qwen 2.5 (0.5B, 1.5B, 3B, 7B, 14B)	29%

Per-model preference for handoff vs. peak extraction, grouped by attention paradigm. A model is classed “prefer handoff” when handoff-extraction is the more precise probe on a strict majority (≥ 9 of 17) of the concepts evaluated. phi-2 (Parallel attention) and two Gemma-2 models (Alternating attention) prefer handoff on a majority of concepts but are excluded from the cohort comparison — neither paradigm has sufficient n for generalisation. Full model list in [Henry, 2026b].

MHA is $\sim 3\times$ more likely to favour handoff extraction than GQA at the model level (85% vs. 29%; Fisher’s exact $p = 0.022$), consistent with the cohort-distinction reading developed in the companion validation paper [Henry, 2026c]; the within-cohort exceptions remain real and are not yet mechanistically resolved. An adaptive window-width rule further improves extraction for near-final-layer handoffs (mean $+7.44$ percentage points on triggered cases that improve; 60/79 triggered cases improve (75.9%) in the 23-model primary corpus — see [Henry, 2026b] §5.2 for full details). The GEM ablation protocol — using the handoff layer L_H as the ablation target — is used for causal experiments throughout the companion validation paper [Henry, 2026c]; concept directions in that paper are centroid differences at each layer, not stored GEM settled-direction probes. Delta PCA and Windowed PCA are informative for characterizing assembly dynamics but provide no further gain on downstream ablation tasks.

4.5 Sub-Representations

When a concept’s $S(l)$ curve is multimodal, the `dom_vector` (first principal component of contrastive activations) at each peak defines a distinct linear direction. Empirical measurement across 46 multimodal concept \times model pairs (7 concepts; per-concept N ranges from 2 to 17, full breakdown in Table 5 of [Henry, 2026c]) shows these directions are **geometrically distinct**: per-concept mean cosine between the shallow and deep peak `dom_vectors` falls in the range 0.156–0.433, with the cross-concept average in the 0.2–0.4 band. The range endpoints should be interpreted cautiously for concepts with $N < 5$; the sentiment concept has $N = 2$ and its entry (0.433) reflects only two observations. The two peaks are not the same feature at different amplitudes — they are different linear features that both happen to separate the same contrastive classes.

This implies that a single human concept label (“credibility”, “negation”) maps to **multiple sub-representations** at different processing depths. Interpretive evidence suggests:

- **Shallow sub-representations** form near the embedding layers, likely driven by lexical cues (concept-associated words).
- **Deep sub-representations** form in mid-to-late layers, likely driven by compositional processing (contextual inference, scope, pragmatic reasoning).

The transition between sub-representations at the saddle point is abrupt, not gradual: layer \times layer cosine similarity matrices show block-diagonal structure, and adjacent-layer cosine similarity dips sharply at the saddle point (to as low as 0.35 in some models), indicating a phase transition between distinct encoding regimes.

If sub-representations within a single model are geometrically distinct, the natural next question is whether they correspond *across* models: does a shallow sub-representation in one architecture align with a shallow sub-representation in another, and do deep sub-representations likewise pair? A monolithic single-rotation alignment between architectures would predict no such depth structure; a depth-stratified picture predicts that matched-depth pairs align more strongly than mismatched-depth pairs. This is the testable claim formalized as Prediction 5 (§5.5), where it is the strongest confirmed result of the framework.

5. Testable Predictions

The CAZ framework generates seven predictions that are in principle falsifiable with existing open-weight models and standard interpretability tooling. Predictions were formulated from the theoretical framework prior to running the full analysis pipeline; the broad phenomenon of multimodal allocation was observed early — preliminary profiles showed that some models produce multiple peaks — and this informed the framework’s inclusion of scored detection; but the full quantitative scope (multimodal being the norm rather than the exception, mean 3.4 CAZes per concept per model) was not established until the validation pipeline ran. P4 in particular was formulated under the assumption that single-peak models were the primary case and multimodal profiles were exceptional. The specific directional predictions below were committed before per-concept results were examined. Predictions P1–P7 were pre-specified on 2026-04-05 and published at https://waypoint.henrynet.ca/research/concept-assembly-zone/CAZ_Framework.pdf prior to running the full validation pipeline; they were not submitted to a formal external registry such as OSF. Verdicts were recorded after those analyses ran. Verdicts use three categories: **Supported** (prediction holds), **Partially supported** (direction correct, stated mechanism or magnitude wrong), and **Not supported / Not testable as stated** (specific claim failed or premise invalidated). Findings that emerged from investigating prediction failures — including results that work but were not pre-specified — are reported separately in §5.8 to keep the pre-specified record clean.

5.1 Optimal Ablation Depth

Prediction 1: The suppression-to-damage ratio varies systematically with intervention depth relative to the CAZ.

For a given concept, extract the concept direction at each layer via DoM. Apply orthogonal projection at each layer l independently. Measure: (a) behavioral suppression rate on targeted prompts, (b) KL divergence from the unmodified model on unrelated prompts. Plot the ratio (a)/(b) as a function of layer.

Status: Not supported. The prediction specified mid-CAZ as the optimal intervention point. Empirical results [Henry, 2026c] falsify this: in models with redundant encoding (Pythia, GPT-2, OPT), the concept direction persists throughout the post-allocation residual stream, making suppression layer-invariant; capability damage is lowest at late layers, so the optimal point is *post-CAZ*, not mid-CAZ. The specific claim failed. What investigating the failure revealed — a two-regime encoding structure that the prediction did not anticipate — is reported in §5.8. Note: ablation coverage in this paper is 16 of 34 models; the causal impact range (93–100%) should be read as a result for this subset, not the full corpus. The companion evaluation [Henry, 2026c] covers 26 base models.

5.2 Cross-Architecture CAZ Ordering

Prediction 2: CAZ boundaries are concept-specific but show consistent relative ordering across architectures.

Different concepts should have different CAZ windows within the same model. However, the *relative* ordering of those windows — as a fraction of total model depth — should be consistent across architectures. Absolute depth percentages may be family-specific, but relative concept ordering should be consistent.

Status: Partially supported. The ordering is a statistically significant tendency across 8 architectural families: 100% of base models are positively correlated with the consensus ordering (26/26; median $\tau = 0.473$, $W = 351$ (Wilcoxon signed-rank), $p = 1.49 \times 10^{-8}$; 26 base models, $N = 250$ pairs). Three low- τ models (GPT-2: 0.147, GPT-2-medium: 0.077, Qwen2.5-0.5B: 0.140) confirm the tendency is real but not the stable architectural invariant the prediction claimed. The consensus ordering (shallow \rightarrow deep) spans a syntactic-to-behavioral gradient across 17 concepts from specificity to exfiltration (mean depths 21.8%–84.7%; [Henry, 2026c §3]). Detailed per-model breakdown in [Henry, 2026c].

5.3 CAZ Width and Concept Abstraction

Prediction 3: CAZ width correlates with concept abstraction level.

More abstract concepts (e.g., “trustworthiness,” “moral valence”) should have wider CAZ windows than concrete ones (e.g., “negation,” “plurality”), because abstract concepts require more iterative construction across attention layers. This is testable by comparing $l_{\text{end}} - l_{\text{start}}$ for concepts at different levels of semantic abstraction as operationalized by, for example, depth in WordNet or scores on standard concreteness rating datasets.

Status: Exploratory — see §5.8. With $n = 6$ concepts and a researcher-assigned abstraction ranking, the sample is too small to treat this as a tested prediction; the result is reported in §5.8 as a hypothesis-generating finding.

5.4 Post-CAZ Degradation as Logit Interference

Prediction 4: Post-CAZ re-entanglement correlates with unembedding matrix structure.

The degradation of clean concept geometry in late layers is not noise but a structural consequence of preparing the residual stream for logit projection. Concepts whose associated vocabulary tokens are distributionally similar in the unembedding space—close in embedding distance—should show more post-CAZ degradation than concepts with distributionally distinct vocabulary. This would explain why some concepts retain clean geometry into late layers (their vocabulary is well-separated) while others degrade early (their vocabulary clusters).

Status: Not testable as stated. P4 was formulated before the full quantitative scope of multimodal allocation was established — at that point, multi-peak profiles were seen in some models but not yet known to be the norm. The prediction assumes a single post-CAZ decay region, which is a unimodal premise. Multimodal allocation (mean 3.4 CAZes per concept per model; §6) invalidates that premise: apparent “decay” between peaks is inter-CAZ reallocation, not degradation, so there is no single post-CAZ region against which to evaluate the unembedding correlation. The prediction is not falsified by the data — its precondition is not met. A post-hoc analysis prompted by this failure is reported in §5.8.

5.5 Depth-Stratified Representational Convergence

Prediction 5: Cross-architecture alignment is depth-matched.

When a concept has multiple allocation regions, the sub-representation at a given processing depth should align more strongly with the corresponding-depth sub-representation in other architectures than with a different-depth sub-representation. Specifically, after Procrustes rotation, $\text{cosine}(\text{shallow_A}, \text{shallow_B}) > \text{cosine}(\text{shallow_A}, \text{deep_B})$ and $\text{cosine}(\text{deep_A}, \text{deep_B}) > \text{cosine}(\text{deep_A}, \text{shallow_B})$.

Status: Supported. Dataset note: P5’s evaluation uses the multi-model consensus Rosetta Concept Pairs dataset (14 generator models from Anthropic, Google, OpenAI, and Mistral families; see [Henry, 2026d] §2.2), unlike P1–P4, P6–P7 which use the single-model Claude Sonnet 4.6 concept dataset described in §7. Across 122 same-dimension ordered model pairs \times 7 concepts, 563 of 563 valid trials (of 854; 291 excluded for insufficient concept separation at probe depths) show depth-matched alignment exceeding mismatched at proportional processing depths {0.3, 0.5, 0.7} (matched mean 0.353, mismatched 0.199, $\Delta = +0.154$, bootstrap 95% CI [0.147, 0.162], 10,000 bootstrap samples). The 563/563 count and bootstrap CI are the primary evidence; Mann-Whitney $p = 4.8 \times 10^{-229}$ treats trials as independent and is approximate due to within-cluster correlation. A family-stratified analysis of the no-rotation condition [Henry, 2026d] establishes the structure of this depth signal: for cross-family model pairs, the no-rotation condition yields $\Delta \approx 0$ (53.5% positive, chance-level); within-family pairs show $\Delta = +0.347$ (93.2% positive), reflecting shared training dynamics rather than cross-architecture convergence. The cross-family depth-stratification signal requires Procrustes coordinate alignment — it is not detectable without it. Analysis is zero-PCA Procrustes on same-dimension pairs only; full methodology and null-test details are reported in [Henry, 2026d], published simultaneously with this work.

5.6 Lexical vs. Compositional Sub-Representations

Prediction 6: Shallow peaks encode lexical features; deep peaks encode compositional features.

The `dom_vector` at the shallow allocation peak should correlate with token embedding vectors for concept-associated words (e.g., “reliable”, “dubious” for credibility). The `dom_vector` at the deep peak should show lower correlation with token embeddings and higher dependence on multi-token contextual patterns.

Status: Not supported. Token embedding probing (cosine similarity between peak `dom_vectors` and concept-relevant token embeddings) yields near-zero values (~ 0.02) at both peaks, with no significant difference (Wilcoxon $p = 0.82$). Neither peak resembles raw token embeddings. The lexical/compositional distinction may operate at a higher level of abstraction than direct embedding alignment — the shallow feature could depend on token identity through multi-layer composition rather than literally pointing toward any single token’s embedding vector. Requires alternative experimental designs: per-token position attribution, attention knockout, or probing classifiers trained at each peak.

5.7 Multi-Modality as Architectural Property

Prediction 7: Multi-modality prevalence is determined by architecture, not scale.

The fraction of concepts showing multimodal $S(l)$ curves should vary more between architectural families (attention mechanism, activation function, training data) than between scales within a

family.

Status: Indeterminate. The scale correlation is near zero ($\rho = 0.11$, $p \approx 0.63$, two-tailed Pearson; p is approximate because n is approximate), but with $n \approx 26$ the test is underpowered — the 95% CI for ρ includes values up to ~ 0.47 , so absence of a significant correlation is not evidence for the prediction. The qualitative family-level differences are real (Qwen 2.5: deep prominent bimodality, valley depths 26–36%; Gemma 2: subtle structure below the 10% prominence threshold), but these are descriptive observations, not a formal test. Resolving P7 requires either a within-family scale ladder of at least ~ 8 model sizes (the current Pythia ladder of 7 sizes is at the boundary of usefulness) or a formally pre-registered architecture-level test against a formal alternative; both are open work [Henry, 2026c].

5.8 Findings beyond the predictions

Three results emerged from investigating prediction failures or were not pre-specified. They are reported here separately to distinguish hypothesis-driven from data-driven findings.

Two-regime encoding structure (from investigating P1).

P1 predicted mid-CAZ ablation would be optimal; it was not. Investigating why revealed a confound the prediction did not anticipate: encoding strategy. In models with redundant encoding (Pythia, GPT-2, OPT), the concept direction persists throughout the post-allocation residual stream, making suppression layer-invariant; capability damage is lowest at late layers, pushing the optimal intervention point to post-CAZ. In models with sparse encoding (Qwen, Gemma), layer specificity is greater and CAZ location matters more. This is a productive falsification: the two-regime model is more explanatorily complete than the original prediction, and the CAZ profile predicts which regime applies before ablation is run [Henry, 2026c].

Chain-depth decay signal (post-hoc analysis prompted by P4).

P4’s precondition — a single post-CAZ decay region — does not hold under multimodal allocation. After establishing this, we examined a redefined target: degradation from the *final* CAZ peak to the last layer. This post-hoc analysis finds that remaining depth predicts decay ($r = -0.312$, $p < 0.001$, 182 measurements, 26 models [Henry, 2026c]) and unembedding token clustering shows a weak but significant effect ($r = 0.173$, $p = 0.019$). These results are consistent with the intuition behind P4 and are reported here as exploratory findings; they do not rescue P4 as stated.

Width-abstraction correlation (P3, exploratory).

Operationalization note: §5.3 proposed operationalizing “abstraction level” via depth in WordNet or scores on standard concreteness rating datasets. The executed test uses a researcher-assigned abstraction ranking instead. The proposed external validation (WordNet depth or concreteness ratings) was not carried out; the ranking was established by the author before examining per-concept widths.

Excluding credibility (bimodal, high variance), CAZ width correlates with researcher-assigned abstraction rank across the remaining 6 concepts ($r = 0.294$, $p = 0.003$, $n = 132$ concept-model pairs); affective and epistemic concepts show wider CAZes than relational and syntactic ones [Henry, 2026c]. The abstraction ranking was established before examining per-concept widths. **Note on degrees of freedom:** the predictor (researcher-assigned abstraction rank) has only 6 unique values — one per concept, repeated across models. Standard Pearson SE treats $n = 132$ as if all predictor values are independent, but the effective n for the predictor dimension is 6; the p -value is

conservative relative to standard Pearson ($p \approx 0.0005$ at $n = 132$, $r = 0.294$) and was computed via permutation test on concept-level means, which respects the true predictor structure. With $n = 6$ this is underpowered as a prediction test and better read as a hypothesis: a pre-registered replication with a validated concreteness scale would be definitive; the full 17-concept activation corpus (43 models) is available at the Rosetta Activations dataset [Henry, 2026] and supports this test as soon as an external abstraction ranking is established.

6. Proof of Concept

To demonstrate that the CAZ metrics and detection methods produce meaningful results, we present a minimal example on GPT-2-XL (48 layers, 1.5B parameters) using 7 concepts with 250 contrastive pairs each.

6.1 CAZ Detection

The separation curve $S(l)$ for credibility in GPT-2-XL peaks at layer 29 (60% depth) with $S = 1.05$ — the strongest signal among the 7 concepts tested (N=250 contrastive pairs per concept, $k = 2$ smoothing, final-token probing). The scored detector identifies 2 CAZes for this concept under default detection settings (0.5% prominence floor, 3% valley-merge threshold; §4.3): a strong early CAZ at L9 (19%, score=0.20) and the dominant peak at L29 (60%, strong, score=0.37).

Across all 7 concepts in this single model, dominant allocation peaks span 35–60% depth (negation L17, temporal_order L21, certainty and moral_valence L23, sentiment L24, causation L25, credibility L29). Negation has two detected strong CAZes at L13 (28%, score=0.44) and L17 (35%, score=0.38), reflecting the shallow-to-deep sub-representation transition described in §4.5; causation similarly splits across a shallow region near L13 and its dominant peak at L25. The tendency for syntactic and relational concepts to peak earlier than epistemic ones holds — consistent with the cross-architecture ordering tendency reported as P2 (§5.2, Partially supported).

6.2 Scored Detection Reveals Hidden Structure

Lowering the detection threshold from 10% to 0.5% (scored detection) increases the number of detected CAZes from 7 to 10 in this single model — credibility, negation, and causation each reveal secondary allocation regions invisible under the 10% threshold. The additional regions are not noise: ablation across models with full coverage confirms causal impact in 93–100% of cases for detected gentle CAZes [Henry, 2026c], and the additional CAZes here correspond to interpretable sub-representation transitions (§4.5). GPT-2-XL is not the richest example of multimodal structure; models with more pronounced allocation dynamics (e.g., Pythia-160M, which shows a mean of 3.0 CAZes per concept across the 7 evaluated concepts) provide more vivid demonstrations — and the full cross-model pattern is reported in [Henry, 2026c]. Whether regions below the 0.5% floor are also causally active remains untested.

6.3 Scope of Validation

The framework has been validated across 34 models from 8 architectural families (Pythia, GPT-2, OPT, Qwen 2.5, Gemma 2, Llama 3.2, Mistral, Phi) spanning 70M to 12B parameters. Full empirical results — including multi-family scale ladders, structural analysis, cross-architecture alignment, and

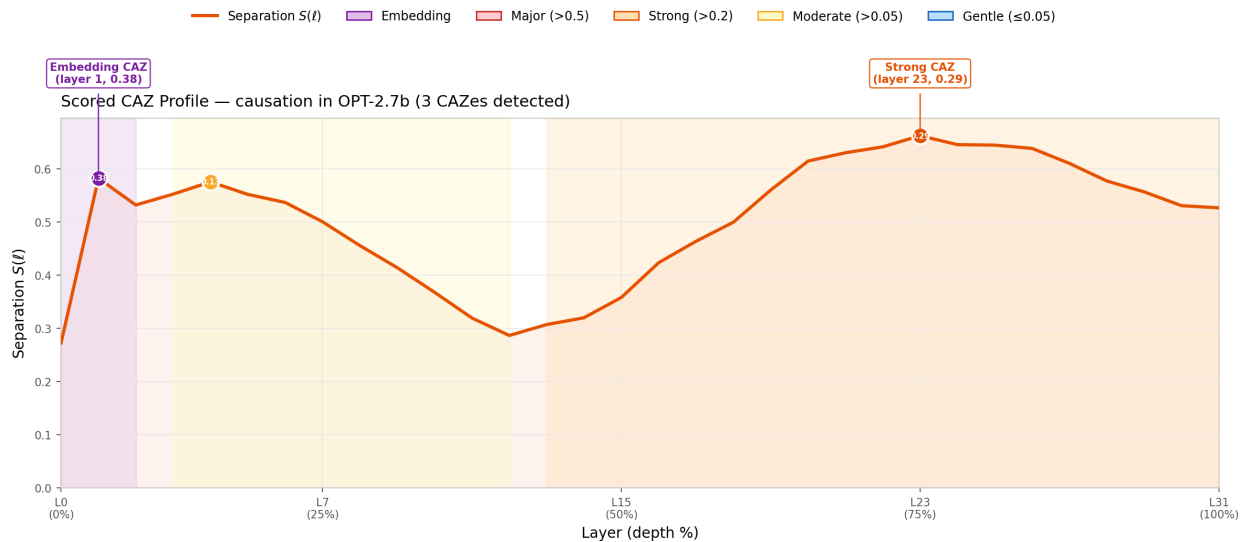


Figure 2: Scored CAZ profile for causation in OPT-2.7B (32 layers). Three CAZes detected: an embedding CAZ at layer 1 (score 0.38) driven by token-level features, and two active CAZes at mid-to-late depth including a strong CAZ near layer 23 (score 0.29). Demonstrating cross-architecture generalization of the scored detector: multi-depth allocation structure is visible in an OPT-family model, a different architectural family and concept than Figure 1. OPT-family models characteristically show fewer, more concentrated CAZes than architectures with alternating or grouped attention — both patterns are detected correctly by the scored detector. $N=250$ contrastive pairs, $k = 1$ smoothing (32 layers), final-token probing, scored detection defaults.

dark matter quantification — are reported in the companion validation paper [Henry, 2026c]. The reference implementation is provided as `rosetta_tools v1.3.1` [Henry, 2026].

7. Limitations

Known limitations include:

Synthetic contrastive data bias

This is the most significant limitation of the current work. All 7 concept datasets used for validation were generated by a single model (Claude Sonnet 4.6). Every CAZ location, every separation score, and every cross-architecture alignment number in this paper is measured against Claude’s definition of each concept. If Claude’s concept boundaries differ systematically from a human consensus definition, then what we are mapping is Claude’s ontology projected onto other models, not a universal property of the models themselves. Multi-model consensus pair generation is addressed in the companion validation paper: Henry [2026c] §C replicates the peak-depth analysis using $\sim 1,400$ pairs per concept generated by 14 models across Anthropic, Google, OpenAI, and Mistral, finding that concept ordering is preserved across all four test architectures. The framework methodology is independent of the data source; only the specific empirical results are at risk.

Model scale

Initial analysis was conducted on NVIDIA L4 GPUs (22 GiB VRAM); full-corpus validation at $N=250$ was completed on NVIDIA H200 hardware, extending coverage to Pythia-12B, Gemma-2-9B, and Llama-3.1-8B that were deferred from the original L4 runs. Frontier-scale models (70B+) were not evaluated; whether CAZ structure and the depth-ordering predictions hold at that scale is an open question.

Smoothing sensitivity

CAZ boundary detection depends on the smoothing parameter k and threshold θ_+ . The current heuristic ($k = \lfloor L/24 \rfloor$) produces consistent results across 34 models but has not been formally validated against ground-truth concept boundaries.

Linearity assumption

The separation metric assumes the concept manifold is approximately linearly separable. For concepts with curved or multi-dimensional structure [Gurnee et al., 2026; Engels et al., 2025b], kernel-based or topological metrics may be required. This limitation is shared with most of the current interpretability literature.

Token position dependence

The framework probes a single fixed token position (the final token by default) and treats the resulting layer-wise separation curve as representative of the concept. Zhao et al. [2025] demonstrate this directly for safety-relevant concepts: harmfulness encodes at the last instruction token while refusal encodes at the last post-instruction token — distinct positions for distinct concepts within the same prompt. CAZ boundaries derived from a single fixed token position may not generalise to concepts that encode elsewhere. No systematic sensitivity analysis on alternate token positions was conducted in this work; this is a known gap rather than an oversight, and position-varied replication is a concrete direction for follow-up.

Scope: semantic concepts only

The CAZ framework applies to concepts that are assembled through transformer layers via the allocation dynamics described here. Tokenization-level concepts — representations tied to byte-level patterns, script detection, BPE boundary artifacts, or sub-word orthography — do not undergo CAZ assembly in the same sense: they are largely established at the embedding layer and do not exhibit the velocity peaks, saddle-point transitions, or cross-architecture alignment that define the CAZ phenomenon. All seven concepts in the current validation corpus (credibility, certainty, causation, temporal_order, sentiment, negation, moral_valence) are semantic, and the universality claims in this paper are scoped to that class. Extending CAZ analysis to tokenization-level representations requires a separate treatment of how such features behave under the layer-indexed metrics defined in §3.2.

Causal validation coverage

Ablation testing in this paper covers 16 of 34 models; the companion validation paper [Henry, 2026c] extends ablation coverage to all 26 base models and confirms that 93–100% of gentle CAZes exceed the non-CAZ ablation baseline. The 8 instruct-tuned variants in this paper’s corpus are not covered by [Henry, 2026c]’s base-model ablation sweep.

PRH measurement sensitivity

Cross-architecture alignment numbers are highly sensitive to the rotation estimation method. PCA compression to low-dimensional subspaces (e.g., $k = 20$) inflates alignment scores: random vectors projected to a 20-dimensional subspace are nearly orthogonal, and Procrustes can achieve near-perfect alignment for arbitrary vector pairs in this setting. The zero-PCA cross-family same-dimension estimate is 0.9805 ± 0.0373 across 17 concepts (1,766 pairs, 33 models, 10 families) against a permuted-label null of $+0.0001$ (grand mean, 17 concepts, 118 pairs; [Henry, 2026d §3.2]). Cross-dimension comparisons using PCA projection should not be used as primary PRH evidence.

SAE residual cross-validation

Section 1 notes that CAZ regions may correspond to SAE dark matter — structured residuals that resist linear decomposition at a fixed layer [Engels et al., 2025a]. The mechanism is plausible: in-progress concept construction within a CAZ produces transitional representations that are neither the input feature nor the output feature. This hypothesis has not been tested in this work. Direct cross-validation — measuring whether gentle CAZ layers predict elevated SAE unexplained residual in the same model — is a concrete open direction.

8. Conclusion

The Concept Allocation Zone framework provides a methodology for tracking how concepts form across transformer depth — complementing the “best layer” view with a dynamical view of concept allocation.

The key contributions are:

1. **Three layer-wise metrics** (Separation, Coherence, Velocity) that characterize concept formation as a process, not a point.
2. **Scored detection** that reveals a spectrum of allocation regions from major to gentle, replacing binary thresholds with continuous scoring.

3. **The CAZ-is-not-a-concept distinction** — CAZes are depth-localized allocation regions in which the model organizes geometry to serve concepts. Multiple concepts share CAZes; single concepts participate in multiple CAZes across depth.
4. **Sub-representation tracking** across depth: within-model `dom_` vectors at shallow and deep peaks are geometrically distinct (cosine 0.2–0.4 with block-diagonal cosine similarity structure across layers, §4.5), with cross-architecture depth-matching confirmed under leave-one-concept-out cross-validation (P5).

Verdict definitions. *Supported*: prediction holds. *Partially supported*: direction correct, stated mechanism or magnitude wrong. *Not supported*: specific claim failed. *Not testable as stated*: prediction’s precondition invalidated by the data. *Exploratory*: result exists but sample too small to constitute a test. Results arising from investigating prediction failures are in §5.8, not this table.

#	Prediction	Verdict
P1	Mid-CAZ ablation yields optimal suppression-to-damage ratio	Not supported
P2	CAZ boundaries show consistent relative ordering cross-architecture	Partially supported
P3	CAZ width correlates with abstraction level	Exploratory†
P4	Post-CAZ degradation correlates with unembedding matrix structure	Not testable as stated‡
P5	Cross-architecture alignment is depth-matched	Supported§
P6	Shallow peaks encode lexical features; deep peaks encode compositional	Not supported
P7	Multi-modality prevalence is architectural, not scale-dependent	Indeterminate

†See §5.8 (width-abstraction correlation). ‡See §5.8 (chain-depth decay post-hoc analysis). §563/563 same-dimension trials positive, $\Delta=+0.154$, bootstrap 95% CI [0.147, 0.162]; Mann-Whitney $p = 4.8 \times 10^{-229}$ approximate due to within-cluster correlation — the trial count and CI are the primary evidence. Full methodology in [Henry, 2026d].

The framework’s strongest empirical result is P5. Its evidential base is 122 same-dimension model pairs contributing 563 valid depth-fraction comparisons (of 854), not 563 independent observations; the 563/563 positive trial count and bootstrap CI are the primary summary of effect consistency, and the Mann-Whitney p-value is approximate due to within-cluster correlation. The most consequential revision the data required is the replacement of the single-peak assumption with multi-peak allocation — a falsification of P4’s premise that strengthened the framework’s explanatory scope. Full empirical results are reported in [Henry, 2026c].

The reference implementation is available as `rosetta_tools v1.3.1` [Henry, 2026], an open-source Python library providing the full CAZ extraction, alignment, ablation, and feature tracking pipeline described in this paper. All code, data, and analysis scripts for this paper series are available at <https://github.com/jamesrahenry/Rosetta>. Pre-extracted model activations for all corpus models across 17 concepts are available as the Rosetta Activations dataset at <https://huggingface.co/datasets/james-ra-henry/Rosetta-Activations>.

Acknowledgments

The author acknowledges the support of TELUS, specifically the Chief AI Office, the AI Accelerator, and the Chief Security Office.

Thanks to Ivey Chiu, Steve Pearson, and Krista Hickey for helpful discussions and guidance.

The author acknowledges computational and academic support from the Vector Institute for Artificial Intelligence.

Thanks to Ilya Grishchenko and David Lie (University of Toronto) for helpful discussions.

Claude (Anthropic) contributed substantially to this work. Specifically: iterative discussion of validation methodology design (null experiment selection, the split-calibration construction-artifact test); manuscript drafting and structural editing; and code review for the rosetta_tools extraction pipeline. The framework’s predictions (§5), the decision to use zero-PCA Procrustes as the primary alignment method, and all final interpretive judgements were made by the author.

References

- Arditi, A., Obeso, O., Syed, A., Paleka, D., Panickssery, N., Gurnee, W., & Nanda, N. (2024). Refusal in language models is mediated by a single direction. *arXiv preprint arXiv:2406.11717*. <https://arxiv.org/abs/2406.11717>
- Alain, G., & Bengio, Y. (2017). Understanding intermediate layers using linear classifier probes. *arXiv preprint arXiv:1610.01644*. <https://arxiv.org/abs/1610.01644>
- Belinkov, Y. (2022). Probing classifiers: Promises, shortcomings, and advances. *Computational Linguistics*, 48(1), 207–219.
- Belrose, N., Ostrovsky, I., McKinney, L., Furman, Z., Smith, L., Halawi, D., Biderman, S., & Steinhardt, J. (2023). Eliciting latent predictions from transformers with the tuned lens. *arXiv preprint arXiv:2303.08112*. <https://arxiv.org/abs/2303.08112>
- Bishop, C. M. (2006). *Pattern Recognition and Machine Learning*. Springer.
- Bricken, T., Templeton, A., Batson, J., Chen, B., Jermyn, A., Conerly, T., Turner, N., Anil, C., Denison, C., Askell, A., Lasenby, R., Wu, Y., Kravec, S., Schiefer, N., Maxwell, T., Joseph, N., Tamkin, A., Nguyen, K., McLean, B., Burke, J. E., Hume, T., Carter, S., Henighan, T., & Olah, C. (2023). Towards monosemanticity: Decomposing language models with dictionary learning. *Transformer Circuits Thread*, Anthropic. <https://transformer-circuits.pub/2023/monosemantic-features/index.html>
- Chan, L., Garriga-Alonso, A., Goldowsky-Dill, N., Greenblatt, R., Nitishinskaya, J., Radhakrishnan, A., Shlegeris, B., & Thomas, N. (2022). Causal scrubbing: A method for rigorously testing interpretability hypotheses. *AI Alignment Forum*, December 2022. <https://www.alignmentforum.org/posts/JvZhhzycHu2Yd57RN/causal-scrubbing-a-method-for-rigorously-testing>
- Cunningham, H., Ewart, A., Riggs, L., Huben, R., & Sharkey, L. (2023). Sparse autoencoders find highly interpretable features in language models. *arXiv preprint arXiv:2309.08600*. <https://arxiv.org/abs/2309.08600>

- Elhage, N., Nanda, N., Olsson, C., Henighan, T., Joseph, N., Mann, B., Askell, A., Bai, Y., Chen, A., Conerly, T., DasSarma, N., Drain, D., Ganguli, D., Hatfield-Dodds, Z., Hernandez, D., Jones, A., Kernion, J., Lovitt, L., Ndousse, K., Amodei, D., Brown, T., Clark, J., Kaplan, J., McCandlish, S., & Olah, C. (2021). A mathematical framework for transformer circuits. *Transformer Circuits Thread*, Anthropic. <https://transformer-circuits.pub/2021/framework/index.html>
- Engels, J., Riggs, L., & Tegmark, M. (2025a). Decomposing the dark matter of sparse autoencoders. *Transactions on Machine Learning Research (TMLR)*, April 2025. *arXiv preprint arXiv:2410.14670*. <https://arxiv.org/abs/2410.14670>
- Engels, J., Michaud, E. J., Liao, I., Gurnee, W., & Tegmark, M. (2025b). Not all language model features are one-dimensionally linear. *Proceedings of the International Conference on Learning Representations (ICLR 2025)*. *arXiv preprint arXiv:2405.14860*. <https://arxiv.org/abs/2405.14860>
- Mahalanobis, P. C. (1936). On the generalized distance in statistics. *Proceedings of the National Institute of Sciences of India*, 2(1), 49–55.
- Meng, K., Bau, D., Andonian, A., & Belinkov, Y. (2022). Locating and editing factual associations in GPT. *Advances in Neural Information Processing Systems (NeurIPS 2022)*, 35, 17359–17372. *arXiv preprint arXiv:2202.05262*. <https://arxiv.org/abs/2202.05262>
- nostalgebraist. (2020). Interpreting GPT: The logit lens. *LessWrong / AI Alignment Forum*, August 2020. <https://www.lesswrong.com/posts/AcKRB8wDpdaN6v6ru/interpreting-gpt-the-logit-lens>
- Henry, J. (2026). rosetta_tools (v1.3.1). Zenodo. <https://doi.org/10.5281/zenodo.20361433>
- Henry, J. (2026). Rosetta Activations: Pre-extracted transformer residual stream activations for 33 language models across 17 concepts. HuggingFace. <https://huggingface.co/datasets/james-ra-henry/Rosetta-Activations>
- Henry, J. (2026b). Geometric Evolution Maps: Extracting Stable Concept Probes from Transformer Residual Streams. *arXiv preprint*.
- Henry, J. (2026c). Concept Encoding Strategies Across 26 Transformers: A Concept Allocation Zone Evaluation. *arXiv preprint*.
- Henry, J. (2026d). Concept-Selective Convergence: Cross-Architecture Evidence for the Platonic Representation Hypothesis via Zero-PCA Procrustes Alignment. *arXiv preprint*.
- Huh, M., Cheung, B., Wang, T., & Isola, P. (2024). Position: The Platonic Representation Hypothesis. *Proceedings of the International Conference on Machine Learning (ICML 2024)*. *arXiv preprint arXiv:2405.07987*. <https://arxiv.org/abs/2405.07987>
- Kornblith, S., Norouzi, M., Lee, H., & Hinton, G. (2019). Similarity of neural network representations revisited. *Proceedings of the International Conference on Machine Learning (ICML 2019)*, 3519–3529.
- Fisher, R. A. (1936). The use of multiple measurements in taxonomic problems. *Annals of Eugenics*, 7(2), 179–188.
- Geva, M., Schuster, R., Berant, J., & Levy, O. (2021). Transformer feed-forward layers are key-value memories. *Proceedings of the 2021 Conference on Empirical Methods in Nat-*

ural Language Processing (EMNLP 2021), 5484–5495. *arXiv preprint arXiv:2012.14913*. <https://arxiv.org/abs/2012.14913>

- Geva, M., Caciularu, A., Wang, K. R., & Goldberg, Y. (2022). Transformer feed-forward layers build predictions by promoting concepts in the vocabulary space. *Proceedings of the 2022 Conference on Empirical Methods in Natural Language Processing (EMNLP 2022)*, 30–45. *arXiv preprint arXiv:2203.14680*. <https://arxiv.org/abs/2203.14680>
- Goldowsky-Dill, N., MacLeod, C., Sato, L., & Arora, A. (2023). Localizing model behavior with path patching. *arXiv preprint arXiv:2304.05969*. <https://arxiv.org/abs/2304.05969>
- Gurnee, W., Horsley, T., Guo, Z. C., Kheirkhah, T. R., Sun, Q., Hathaway, W., Nanda, N., & Bertsimas, D. (2024). Universal neurons in GPT2 language models. *Transactions on Machine Learning Research (TMLR)*. *arXiv preprint arXiv:2401.12181*. <https://arxiv.org/abs/2401.12181>
- Gurnee, W., Ameisen, E., Kauvar, I., Tarng, J., Pearce, A., Olah, C., & Batson, J. (2026). When models manipulate manifolds: The geometry of a counting task. *Transformer Circuits Thread*, Anthropic. *arXiv preprint arXiv:2601.04480*. <https://arxiv.org/abs/2601.04480>
- Sofroniew, N., Kauvar, I., Saunders, W., Chen, R., Henighan, T., Hydrie, S., Citro, C., Pearce, A., Tarng, J., Gurnee, W., Batson, J., Zimmerman, S., Rivoire, K., Fish, K., Olah, C., & Lindsey, J. (2026). Emotion concepts and their function in a large language model. *Transformer Circuits Thread*, Anthropic. *arXiv preprint arXiv:2604.07729*. <https://arxiv.org/abs/2604.07729>
- Vig, J., Gehrmann, S., Belinkov, Y., Qian, S., Nevo, D., Singer, Y., & Shieber, S. (2020). Investigating gender bias in language models using causal mediation analysis. *Advances in Neural Information Processing Systems (NeurIPS 2020)*, 33, 12388–12401.
- Wang, K., Variengien, A., Conmy, A., Shlegeris, B., & Steinhardt, J. (2023). Interpretability in the wild: A circuit for indirect object identification in GPT-2 small. *Proceedings of the International Conference on Learning Representations (ICLR 2023)*. *arXiv preprint arXiv:2211.00593*. <https://arxiv.org/abs/2211.00593>
- Wollschläger, T., Elstner, J., Geisler, S., Cohen-Addad, V., Günnemann, S., & Gasteiger, J. (2025). The geometry of refusal in large language models: Concept cones and representational independence. *Proceedings of Machine Learning Research (ICML 2025)*, 267, 66945–66970. *arXiv preprint arXiv:2502.17420*. <https://arxiv.org/abs/2502.17420>
- Zhao, J., Huang, J., Wu, Z., Bau, D., & Shi, W. (2025). LLMs encode harmfulness and refusal separately. *arXiv preprint arXiv:2507.11878*. <https://arxiv.org/abs/2507.11878>
- Zou, A., Phan, L., Chen, S., Campbell, J., Guo, P., Ren, R., Pan, A., Yin, X., Mazeika, M., Dombrowski, A.-K., Goel, S., Li, N., Byun, M. J., Wang, Z., Mallen, A., Basart, S., Koyejo, S., Song, D., Fredrikson, M., Kolter, J. Z., & Hendrycks, D. (2023). Representation engineering: A top-down approach to AI transparency. *arXiv preprint arXiv:2310.01405*. <https://arxiv.org/abs/2310.01405>